ACCOUNTS of chemical research

Article

pubs.acs.org/accounts

Boron: Enabling Exciting Metal-Rich Structures and Magnetic Properties

Jan P. Scheifers,[#] Yuemei Zhang,[#] and Boniface P. T. Fokwa*

Departments of Chemistry, University of California Riverside (UCR), Riverside, California 92521, United States

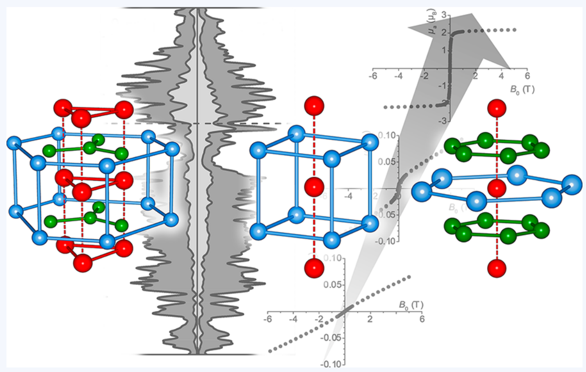

CONSPECTUS: Boron's unique chemical properties and its reactions with metals have yielded the large class of metal borides with compositions ranging from the most boron-rich YB_{66} (used as monochromator for synchrotron radiation) up to the most metal-rich $Nd_2Fe_{14}B$ (the best permanent magnet to date). The excellent magnetic properties of the latter compound originate from its unique crystal structure to which the presence of boron is essential. In general, knowing the crystal structure of any given extended solid is the prerequisite to understanding its physical properties and eventually predicting new synthetic targets with desirable properties. The ability of boron to form strong chemical bonds with itself and with metallic elements has enabled us to construct new structures with exciting properties. In recent years, we have discovered new boride structures containing some unprecedented boron fragments (trigonal planar B_4 units, planar B_6 rings) and low-dimensional substructures of magnetically active elements (ladders, scaffolds, chains of triangles). The new boride structures have led to new superconducting materials (e.g., NbRuB) and to new itinerant magnetic materials (e.g., $Nb_6Fe_{1-x}Ir_{6+x}B_8$). The study of boride compounds containing chains (Fe-chains in antiferromagnetic $Sc_2FeRu_5B_2$), ladders (Fe-ladders in ferromagnetic $Ti_9Fe_2Rh_{18}B_8$), and chains of triangles (Cr_3 chains in ferrimagnetic and frustrated $TiCrIr_2B_2$) of magnetically active elements allowed us to gain a deep understanding of the factors (using density functional theory calculations) that can affect magnetic ordering of such low-dimensional magnetic units. We discovered that the magnetic properties of phases containing these magnetic subunits can be drastically tuned by chemical substitution within the metallic nonmagnetic network. For example, the small hysteresis (measure of magnetic energy storage) of $Ti_2FeRh_5B_2$ can be successively increased up to 24-times by gradually substituting Ru for Rh, a result that was even surpassed (up to 54-times the initial value) for Ru/Ir substitutions. Also, the type of long-range magnetic interactions could be drastically tuned by appropriate substitutions in the metallic nonmagnetic network as demonstrated using both experimental and theoretical methods. It turned out that Ru-rich and valence electron poor metal borides adopting the $Ti_3Co_5B_2$ or the Th_7Fe_3 structure types have dominating antiferromagnetic interactions, while in Rh-rich (or Ir-rich) and valence electron rich phases ferromagnetic interactions prevail, as found, for example, in the $Sc_2FeRu_{5-x}Rh_xB_2$ and $FeRh_{6-x}Ru_xB_3$ series.

Fascinatingly, boron clusters (e.g., B_6 rings) even directly interact in some cases with the magnetic subunits, an interaction which was found to favor the Fe–Fe magnetic exchange interactions in the ferromagnetic $Nb_6Fe_{1-x}Ir_{6+x}B_8$.

Using less expensive transition metals, we have recently predicted new itinerant magnets, the experimental proof of which is still pending. Furthermore, new structures have been discovered, all of which are being studied experimentally and computationally with the aim of finding new superconductors, magnets, and mechanically hard materials.

A new direction is being pursued in our group, as binary and ternary transition metal borides show great promise as efficient water splitting electrocatalysts at the micro- and nanoscale.

1. INTRODUCTION

Boron tends, like carbon and silicon, to form covalent molecular, as well as extended compounds, but boron's "electron deficiency" (boron has one less valence electron than the number of valence orbitals) enables the formation of multicenter B–B bonds and therefore unusual molecular and extended structures. Boron reacts with most metals forming metal borides, ranging from the most boron-rich YB_{66} up to the most metal-rich $Nd_2Fe_{14}B$. Presently, more than 1000 binary and ternary borides have been prepared and characterized. They crystallize in well over 150 different structure types.[1−3] A summary of the common synthetic approaches is given in recent reviews.[1,3]

The diversity in compositions and crystal structures of metal borides has yielded a large number of compounds with interesting properties and applications. Due to strong covalent boron–boron and metal–boron bonds in metal borides, they are characterized by high melting points, excellent wear resistance, and chemical inertness.[1−3] Moreover, many boron-rich borides display high stability toward neutron and other

Received: May 26, 2017
Published: August 9, 2017

 © 2017 American Chemical Society

DOI: 10.1021/acs.accounts.7b00268
Acc. Chem. Res. 2017, 50, 2317−2325

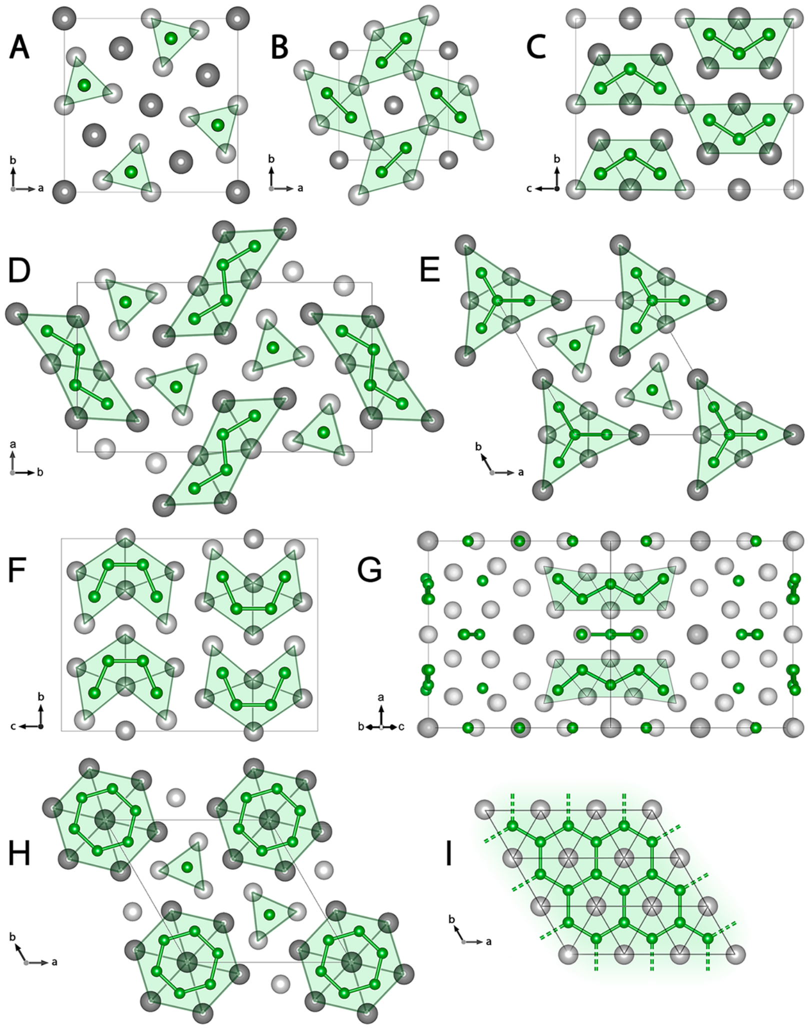

Figure 1. Projections of some boride structures highlighting boron atoms and fragments formed by face-sharing boron-filled trigonal prisms (metals, light and dark gray; boron, green). (A) Isolated boron atoms in $Ti_3Co_5B_2$-type structure. (B) B_2-dumbbells in Mo_2FeB_2-type structure. (C) B_3 fragments in W_3CoB_3. (D) *trans*-B_4 fragments in $Ti_{1+x}Rh_{2-x+y}Ir_{3-y}B_3$. (E) Trigonal planar B_4 unit in $Ti_{1+x}Os_{2-x}RuB_2$-type. (F) *cis*-B_4 fragments in β-Cr_2IrB_2. (G) Zig-zag B_5 units in $Ni_{12}AlB_8$. (H) B_6 rings in $Nb_6Fe_{1-x}Ir_{6+x}B_8$. (I) Infinite honeycomb B-layer in AlB_2-type structure.

types of radiation; for example, single crystals of YB_{66} are used as monochromators for soft synchrotron radiation,[4] while LaB_6 is used as thermionic emitter.[5] Many borides are superconducting materials (e.g., MgB_2, first high-temperature metallic superconductor),[6] while others are magnetocaloric materials (e.g., $AlFe_2B_2$)[7] or magnetic materials (e.g., $Nd_2Fe_{14}B$).[8] The latter compound is probably the most prominent metal boride (known as neodymium magnet), as it is the best permanent magnet to date. Magnetic compounds play a central role in our information society, for example, data storage and retrieval benefit from the exceptional magnetic properties. The high demand has resulted in increased efforts to "design" new magnetic materials with specific properties, which is a rather complicated task, mainly because of the complexity of magnetism itself. In fact, even today, it remains difficult to understand why some materials order magnetically (antiferromagnetism, ferromagnetism, ferrimagnetism, etc.) and others do not (paramagnetism, diamagnetism). The case of pure itinerant magnetism (magnetism solely due to conduction electrons) is particularly intriguing: To date, only three pure itinerant magnets (Sc_3In, $ZrZn_2$, and TiAu) have been found, although there are several thousand intermetallic compounds known.[9] However, the presence of magnetically active 3d elements (Cr, Mn, Fe, Co, Ni) drastically increases the chances for itinerant magnetism, because of the triggering presence of magnetic moments on these elements. The magnetic metal-rich borides covered in this Account fall into this category of itinerant magnetic materials containing magnetically active elements. Our research combines density-functional theory (DFT) calculations and experiments in a synergistic way to explain some unexpected structures or magnetic phenomena on the one side and to discover new phases with potentially interesting magnetic properties on the other.

2. STRUCTURAL VARIATIONS AND CHEMICAL BONDING IN METAL-RICH BORIDES

In many crystal structures of metal-rich borides, the boron atoms are located in trigonal prisms built by metal atoms, but square antiprismatic (e.g., in $CuAl_2$-type borides, boron on the Cu site)[10] and octahedral (e.g., in boride perovskites)[1] boron coordinations also occur. A remarkable and still unique boron environment is the tetragonal prism in $Ti_2Ru_3Ir_2B_3$, where boron-centered trigonal and tetragonal prisms coexist.[11] The trigonal prisms are further connected to each other by sharing

DOI: 10.1021/acs.accounts.7b00268
Acc. Chem. Res. 2017, 50, 2317−2325

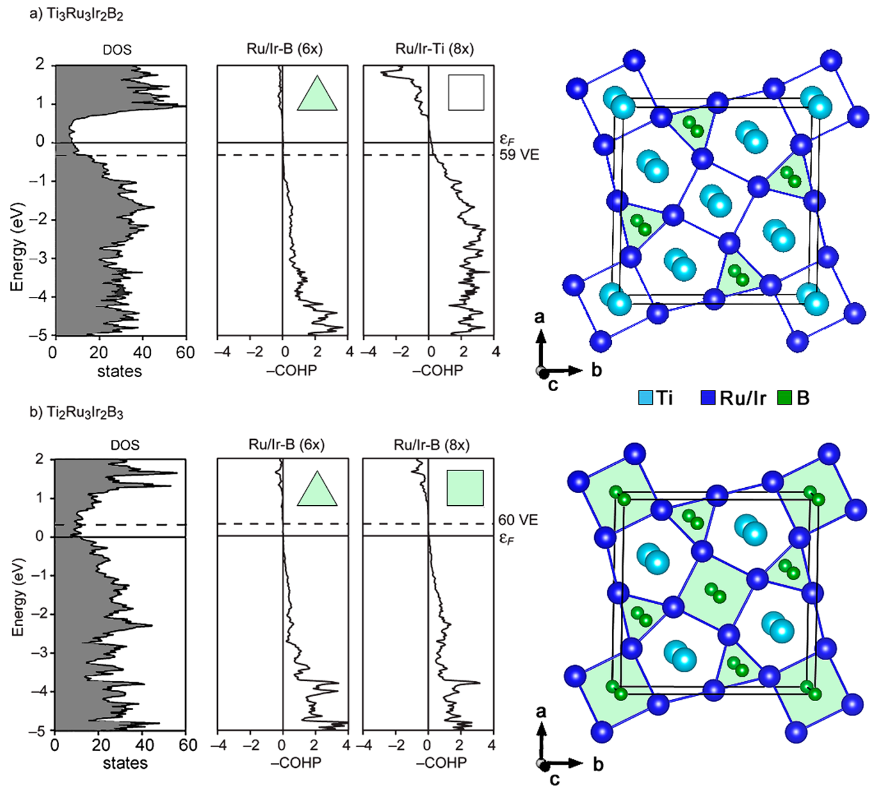

Figure 2. DOS, COHP curves, and crystal structures of $Ti_3Ru_3Ir_2B_2$ and $Ti_2Ru_3Ir_2B_3$.

their corners, edges, or faces to form three-dimensional (3D) frameworks. Typically, the trigonal prisms are stacked on top of each other sharing their triangular faces, thereby creating a layer-like structural arrangement. For example, many ternary (and quaternary) transition metal-rich borides have a layer-like structure, where the electropositive metal atoms and boron are often found in the same layer sandwiched by layers of the electronegative metal. However, strong metal−boron bonds connect the different layers instead of weak van der Waals interactions as in, for example, graphite or MoS_2. Nevertheless, some cases are also known where a single layer accommodates all elements.[12]

Depending on the connection between the boron-centered trigonal prisms (or the other polyhedral types), either the boron atoms are isolated from one another (case of corner- and edge-sharing) or they bond with the neighboring boron atoms to form small boron clusters (case of face-sharing via rectangular faces). In these boron clusters, the short boron−boron distances (ca. 1.7−1.9 Å) usually lead to strong bonding interactions.[1] Several boron clusters have been discovered, ranging from the smallest B_2 dumbbell cluster to the largest B_{20} cage unit. All boron clusters shown in Figure 1 can be considered as building blocks of the boron honeycomb layers found in AlB_2-type structures (Figure 1I). The boron dumbbell is the most common fragment and has been found in many crystal structure types, including the recently discovered NbRuB[13] and Nb_2OsB_2.[14] Angulated B_3 units are reported in W_3CoB_3-type borides.[15] The B_4 cluster is the most versatile, as five different configurations have been reported: the zigzag *trans*-B_4 fragment (found in Mo_2IrB_2,[16] Ni_3ZnB_2,[17] and $Ti_{1+x}Rh_{2-x+y}Ir_{3-y}B_3$[18]), the zigzag *cis*-$B_4$ unit (in β-Cr_2IrB_2),[19] the trigonal planar B_4 fragment (in $Ti_{1+x}Os_{2-x}RuB_2$),[20] the linear B_4 chain (in Rh_5B_4 with unusually large B−B distances),[21] and the rather unique B_4 tetrahedron (in $Ni_{20}AlB_{14}$).[22] The largest boron chain (zigzag B_5 cluster) was recently discovered in $Ni_{12}AlB_8$.[23] Fascinatingly, six boron atoms build a B_6 ring, first discovered in our lab in the boride $Ti_7Rh_4Ir_2B_8$ and later in many related borides.[24−27] Such ring fragments of boron atoms are the most stable entities in the gas phase, where B_n clusters (n = 3−40) have been extensively studied both experimentally and theoretically.[28] Lastly, the boron fragment with the highest number of boron atoms is the B_{20} cage observed for the first time in $Ni_{21}Zn_2B_{24}$.[17]

Generally, there are three types of bonds with varying strengths in metal-rich borides containing boron clusters: B−B, M−B, and M−M (M = metal). There is a common agreement that the chemical bonding in borides involves simultaneous contributions of covalent, metallic, and ionic bonding to the cohesive energy. In molecules, populating antibonding orbitals or vacating bonding orbitals will decrease the orbital overlap population, which in turn destabilizes a molecule (or structure). To identify the overlap populations in solids, tools such as the crystal orbital Hamilton population (COHP) analysis are commonly used.[29] By weighing the density of states (DOS) according to the corresponding element of the Hamiltonian, the band structure energy is partitioned into bonding, nonbonding, and antibonding contributions. The Fermi level (E_F) would ideally coincide with the crossover from antibonding to bonding states, indicating that the interatomic bonding interactions are optimized. For some intermetallic compounds, the occurrence of a pseudogap at E_F in the DOS plot is considered to indicate electronic stability.[30] The presence of a pseudogap typically causes a wide range of nonbonding states around E_F in the COHP curves of the strongest interactions (Figure 2, Ru/Ir−B COHP). Therefore, shifting the Fermi level within this energy range, by variation of

DOI: 10.1021/acs.accounts.7b00268
Acc. Chem. Res. 2017, 50, 2317−2325

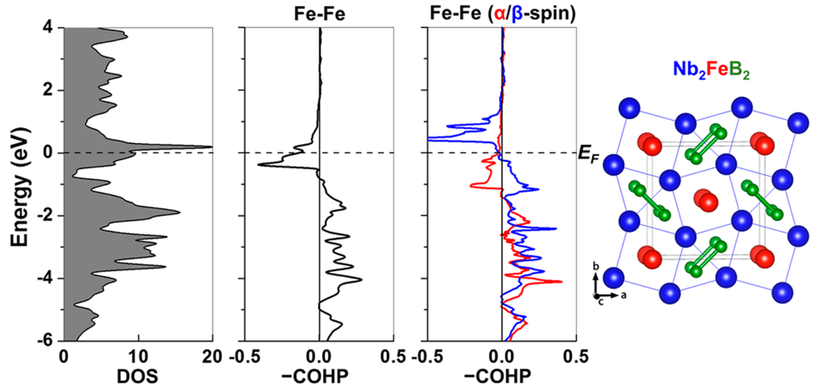

Figure 3. Total DOS, Fe−Fe COHP plots (non-spin-polarized, black; spin-polarized, red/blue), and crystal structure of Nb_2FeB_2.

the valence electron count (VEC) through atomic substitutions, will result in electronically similar phases with nearly the same stability, thus allowing the prediction of stable isotypic compounds and solid solution ranges. We have used this strategy with great success in recent years to not only understand the formation of isotypic phases but also to predict new compounds and exclude the formation of others (see our recent works on NbRuB and derived phases,[13,31] $T_{3-x}Ru_{5+x}B_2$ (T = Zr, Hf),[32] $Ti_7Rh_4Ir_2B_8$,[24] and $Ti_{3-x}Ru_{5-y}Ir_yB_{2+x}$[11]). For example, we could rationalize the formation of unexpected compositions in the complex boride series $Ti_{3-x}Ru_{5-y}Ir_yB_{2+x}$: Starting with $Ti_3Ru_3Ir_2B_2$, the unexpected substitution of one titanium by one boron in a tetragonal prismatic environment leading to $Ti_2Ru_3Ir_2B_3$ could be understood. In fact, the COHP curves (Figure 2) of the strongest interaction (Ru/Ir−B) in $Ti_3Ru_3Ir_2B_2$ and $Ti_2Ru_3Ir_2B_3$ showed large nonbonding areas around E_F indicating not only optimized bonding but also the possibility to shift E_F in this range without destabilizing this interaction. However, analysis of the second most stable interaction (Ru/Ir−Ti) reveals a much smaller range of nonbonding interactions and increasing antibonding states above E_F, making this intermetallic interaction a limiting factor for phase stability. This finding narrowed the VEC range of stability of the complex boride series $Ti_{3-x}Ru_{5-y}Ir_yB_{2+x}$ down to 59−61 VEC (limits determined by the pseudogap and the Ru/Ir−Ti COHP shapes). Consequently, the experimentally obtained four quaternary compositions (for x = 0, 0.37, 0.73, 1) were all predicted to be stable, because the VEC of each of them lies in the above given stable VEC range. These calculations further predict, via the rigid band model (see below for details), that quaternary phases of this complex boride series will be more stable than their ternary counterparts (e.g., "$Ti_2Ru_5B_3$" or "$Ti_3Ru_5B_2$"), because the VECs of the latter all lie outside the predicted range. In fact, none of these ternary phases could be synthesized to date despite several attempts using the same synthetic method employed for the stable quaternaries.

In other cases, the presence of a peak in the DOS at E_F indicates an electronic instability, which could drive an electronic or structural distortion. If the peak at E_F corresponds to strong antibonding M−M (M = magnetically active metal) interactions, it can result in spin-polarization and direct ferromagnetic (FM) M−M interactions. Conversely, when the M−M interactions are nonbonding at E_F, the substance may exhibit antiferromagnetic M−M interactions.[29] For example, the non-spin-polarized electronic structure calculations of Nb_2FeB_2 (Mo_2FeB_2-type structure containing Fe-chains, Figure 3) indicates a relatively high electron density at E_F corresponding mainly to remarkable Fe−Fe antibonding interactions (Figure 3). Accordingly, spin polarization of Nb_2FeB_2[33] leads to the appearance of a pseudogap in the DOS at E_F and a split into majority α- and minority β-spins for Fe, thus minimizing the Fe−Fe antibonding character at E_F (Figure 3). This optimized bonding situation shows that the presence of direct ferromagnetic interaction between the Fe-atoms helped to stabilize this structure. However, the overall magnetic ordering of the compound is predicted to be antiferromagnetic (AFM), because the AFM arrangement among Fe-chains is energetically more favorable than the FM arrangement. Replacing Fe by the higher homologue and "non-magnetic" Ru leads to Nb_2RuB_2.[33] However, Ru undergoes a structural Peierls distortion from equidistant Ru−Ru intrachain contacts to Ru-dumbbells. COHP analysis indicates antibonding interactions at E_F for the equidistant Ru-chain (Figure 4a);

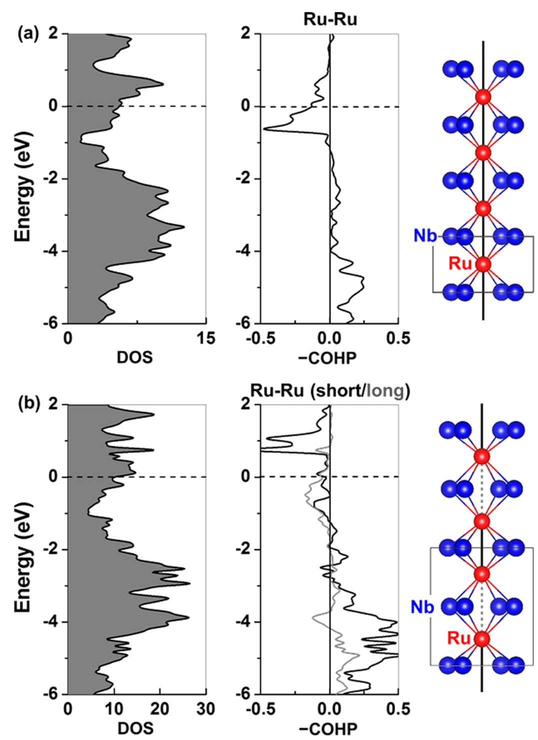

Figure 4. Total DOS and Ru−Ru COHP plots of Nb_2RuB_2 in (a) Nb_2FeB_2-type and (b) Nb_2OsB_2-type structures. Two different Ru chains are depicted on the right.

DOI: 10.1021/acs.accounts.7b00268
Acc. Chem. Res. 2017, 50, 2317−2325

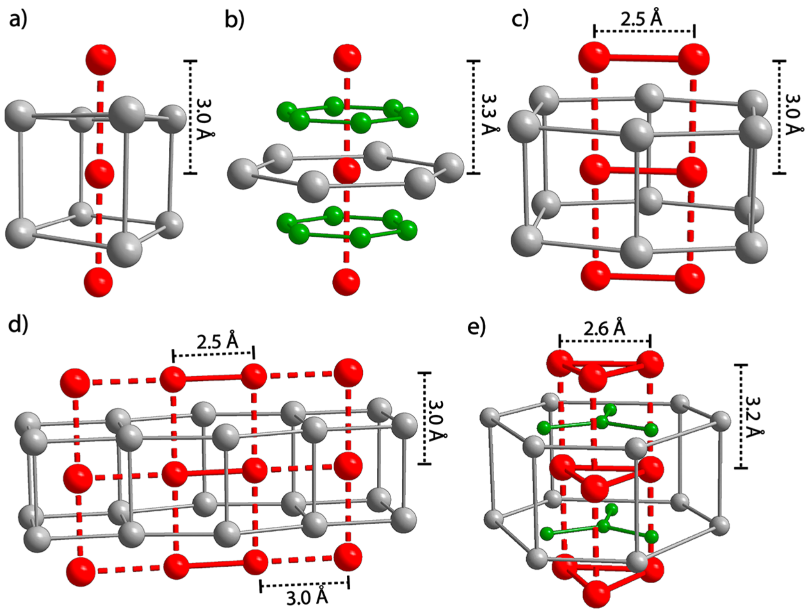

Figure 5. Topologies of low-dimensional magnetic substructures found in the crystal structures of some complex metal-rich borides: (a) chain, as found in Mo_2FeB_2- and $Ti_3Co_5B_2$-type structures; (b) chain imbedded in B_6 rings in $Nb_6Fe_{1-x}Ir_{6+x}B_8$; (c) ladder in $Ti_9Fe_2Ru_{18}B_8$; (d) scaffold in $Ti_8Fe_3Ru_{18}B_8$; (e) chains of Cr-triangles imbedded in B_4 fragments in $TiCrIr_2B_2$.

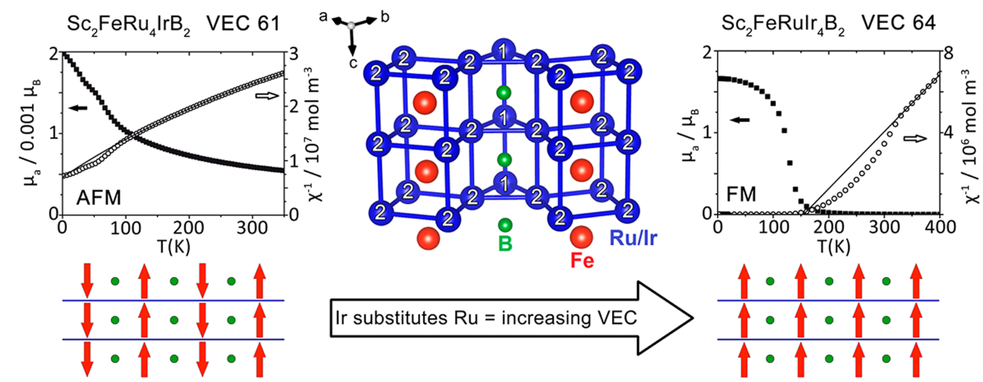

Figure 6. Tuning magnetic properties in the $Sc_2FeRu_{5-x}Ir_xB_2$ series by varying valence electron count (VEC) through substitution of magnetically silent elements. Part of the $Sc_2FeRu_{5-x}Ir_xB_2$ structure (middle, 1 = 2*c* site, 2 = 8*j* site; for unit cell, see Figure 7). Most probable spin arrangements as proposed by DFT total energy calculations (bottom).

however they vanish almost entirely when Ru-dumbbells are formed instead (Figure 4b). Consequently, the crystal structure of Nb_2RuB_2 distorts from the Mo_2FeB_2-type to a new superstructure (Nb_2OsB_2-type) with a doubled unit cell to account for the chain distortion. This behavior was found for several other phases.[14,31,34]

3. TUNING MAGNETIC PROPERTIES BY MODIFYING CRYSTAL AND ELECTRONIC STRUCTURES

The structures of most metal-rich borides we have studied contain low-dimensional subunits of magnetically active elements (Figure 5): chains (e.g., in $Sc_2FeRh_5B_2$ and $Nb_6FeIr_6B_8$), ladders (in $Ti_9Fe_2Ru_{18}B_8$), scaffolds (in $Ti_8Fe_3Ru_{18}B_8$), and chains of triangles (in $TiCrIr_2B_2$).[26,35−37] In many cases, a magnetically inactive element was selectively substituted by a magnetically active 3d metal (Cr, Mn, Fe, or Co), thus enabling long-range magnetic ordering. For example, starting from the ternary nonmagnetic phases $Sc_3Rh_5B_2$,[38] $Ti_{11-x}Ru_{18+x}B_8$,[39] and $Nb_7Ir_6B_8$,[40] the ferromagnets $Sc_2FeRh_5B_2$, $Ti_9Fe_2Ru_{18}B_8$, and $Nb_6FeIr_6B_8$ are "designed" by substituting the nonmagnetic Sc, Ti, and Nb, respectively, with the magnetically active Fe at specific sites in the crystal structures. $Sc_3Rh_5B_2$ belongs to the large group (more than 60 phases known) of $Ti_3Co_5B_2$-type borides, which has produced some of the most exciting magnetic compounds and series. This structure type provides a great deal of possibilities to adjust the electronic structure and to tune the magnetic properties. In fact, by substituting elements in this structure type, the electron count (and the conduction electrons) can be adjusted causing the Fermi-level to shift with respect to a *basically unchanged* band structure (rigid-band model), and consequently affecting the itinerant magnetic properties. We have therefore studied experimentally and theoretically the magnetic properties of these metal-rich borides by changing the VEC while preserving the type and the number of magnetically active element in each series. The first series that enabled a chemical fine-tuning of the magnetic properties was $Sc_2FeRu_{5-x}Rh_xB_2$ (**series 1**, x = 0, 1, ..., 5 with respective VEC = 60, 61, ..., 65). The compositions of **series 1** differ exclusively in the ratio of the magnetically "silent" metals Ru and Rh. Upon varying VEC from 60 to 65

DOI: 10.1021/acs.accounts.7b00268
Acc. Chem. Res. 2017, 50, 2317−2325

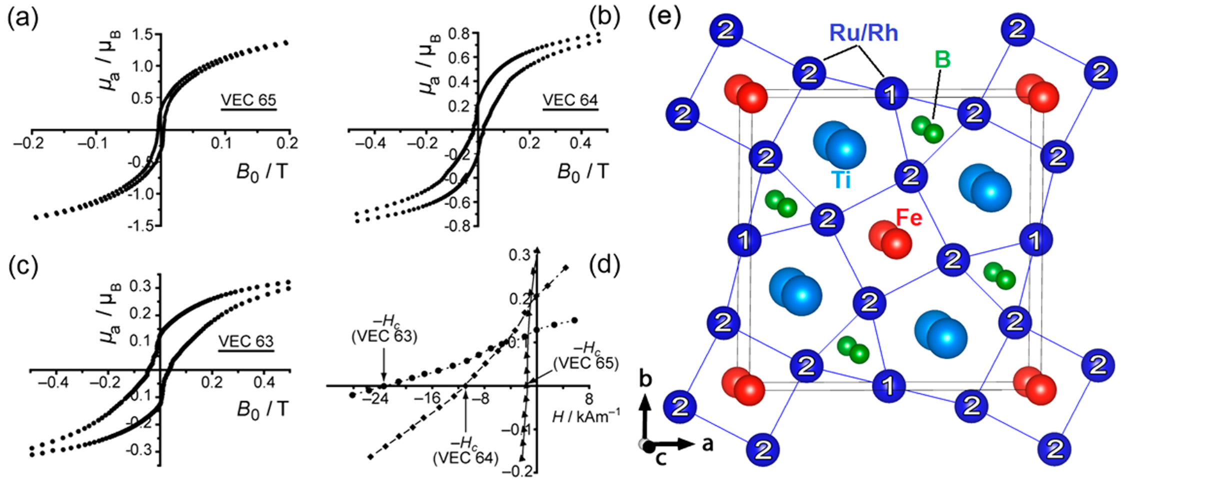

Figure 7. (a–c) Hysteresis loops μ_a vs H [recorded at 5 K] showing their enlargement with decreasing valence electron count (VEC) from 65 to 63 in the $Ti_2FeRu_{5-x}Rh_xB_2$ series. (d) Enlarged left parts of these hysteresis loops showing the increasing coercivity, H_c, with decreasing VEC. (e) Crystal structure of $Ti_2FeRu_{5-x}Rh_xB_2$ (1 = 2*c* site, 2 = 8*j* site).

(increasing Rh content), the stepwise change of long-range magnetic ordering from strong antiferromagnetism (VEC = 60) to strong ferromagnetism (VEC = 65) was observed together with an increase of the magnetic saturation moment in the ferromagnetic range.[35] Based on these experimental data, we could carry out quantum-chemical calculations for **series 1** to understand the changes from antiferromagnetic to ferromagnetic behavior. This theoretical analysis demonstrated a correlation between the effective exchange parameter (J_0) and the VEC in the d-band.[41] The J_0 term is dominated by the iron site and varies from preferred antiferromagnetic coupling below ca. VEC 62 to ferromagnetic coupling above ca. VEC 63. One important theoretical discovery was the significant contributions to the total magnetic moment from the Rh/Ru sites: The (Rh/Ru)−Fe interactions yield leading contributions to the total effective coupling at the Fe atoms (J_{Fe-Fe}). Due to the larger effective exchange parameter J_{Fe-Rh} (3.77 meV) compared to J_{Fe-Ru} (0.07 meV), a greater number of Rh atoms in the vicinity of Fe in the structure should increase the total effective coupling at the Fe atom (J_{Fe-Fe}), which will manifest as larger local magnetic moments on iron. A subsequent theoretical investigation on the influence of Rh or Ir site preference on the magnetic properties of $M_2Fe(Ru_{0.8}T_{0.2})_5B_2$ (M = Sc, Ti, Zr; T = Rh, Ir) phases clearly indicates that substituting Ru by Rh or Ir at the 8*j* site (tetragonal prism around Fe, Figure 6, middle) indeed increases the calculated magnetic moments on the Fe atoms.[42] Single-crystal X-ray diffraction on the $Sc_2FeRu_{5-x}Ir_xB_2$ (x = 1−4) series showed a clear site preference of Ru for site 2*c* and Ir for site 8*j* (Figure 6, middle). The Ir-rich $Sc_2FeRu_2Ir_3B_2$ is important to understand this behavior because it is the only member of the series whose crystal structure indicates a large amount of Ir (65%) on site 8*j* and a large amount of Ru (65%) on site 2*c*. Its magnetic moment (0.45 μ_B) is 5 times larger than the moment found for the one-electron-less (and Ru-rich) $Sc_2FeRu_3Ir_2B_2$ (0.09 μ_B) where Ru is the predominant component on both sites. This clearly indicates that the presence of Ir as the majority component at site 8*j* is the main reason for the drastic increase of the magnetic moment in this series, as predicted. The two remaining members of the quinary series, the most Ru-rich and most Ir-rich members, have the lowest and highest magnetic moments, corresponding to dominating AFM and FM interactions, respectively (see Figure 6). This trend is expected because Ir has one more valence electron than Ru and the amount of Ir in site 8*j* is the lowest in the most Ru-rich member and the highest in the most Ir-rich one. This analysis indicates that the Ru/Ir site preference and the change in VEC are the main reasons for the drastic changes of the magnetic properties along this Ru/Ir-based series.[42]

Another important discovery is the unexpected variation of the hysteresis (via coercive field, H_c) when tuning the magnetic properties of these compounds. This was first observed when studying another series, $Ti_2FeRu_{5-x}Rh_xB_2$ (VEC = 63−67, **series 2**),[44] all members of which were found to order ferromagnetically below their Curie temperatures. Strikingly, they provided the first semihard magnetic borides of transition metals with H_c values up to 23.9 kA/m (see Figure 7) for the VEC 63 phase (for comparison, values below 1 kA/m were recorded in **series 1**).[44] Furthermore, using the 5d element iridium, the highest H_c values measured for transition metal borides so far, up to 52.4 kA/m (for VEC = 63), could be achieved in **series 3** ($Sc_2FeRu_{5-x}Ir_xB_2$).[43] Recently, we investigated theoretically the spin−orbit coupling effect, spin exchange, and magnetic dipole−dipole interactions of these phases, to understand their magnetic anisotropy and to predict new materials with large magnetic anisotropy energy (MAE). Our DFT calculations show that $Sc_2FeRu_3Ir_2B_2$ has by far the largest MAE and strong intra- and interchain Fe−Fe spin exchange coupling, thus confirming its large H_c value. By targeting new compounds containing the earth-abundant and less expensive Co, instead of Rh, Ru, or Ir, we could propose "$Hf_2MnCo_5B_2$" and "$Hf_2FeCo_5B_2$" as potential rare-earth-free, semihard to hard magnetic materials.[45] However, experimental verification is still pending.

In the above-mentioned series, the Fe-chains do not interact with boron atoms. In contrast, we discovered the phase $Nb_6Fe_{1-x}Ir_{6+x}B_8$ recently,[26] which contains Fe-chains embedded in stacked planar B_6 rings.[24] DFT calculations predicted ferromagnetic ordering, and COHP chemical bonding analysis revealed a great synergy between the intrachain Fe−Fe magnetic interactions and the B−B bonding interactions within the B_6 rings. In fact, after spin polarization, the strong ferromagnetic Fe−Fe interactions found in the iron chains induce an unexpected strengthening of the B−B interactions in

DOI: 10.1021/acs.accounts.7b00268
Acc. Chem. Res. 2017, 50, 2317−2325

the B_6 rings, while all other Fe-based interactions weakened. Magnetic measurements then confirmed the predicted ferromagnetic ordering below T_c = 350 K.

Another case of magnetic subunit imbedded in boron fragments is the $Ti_{1+x}Os_{2-x}RuB_2$-type $TiCrIr_2B_2$,[38] which contains in its structure chains of Cr_3 triangles interacting with trigonal planar B_4 clusters (see Figure 5e). Triangular arrangements of magnetically active elements are known to induce magnetic frustration in molecular as well as in extended solids,[46] making this new phase a potential candidate for magnetic frustration. Magnetization measurements revealed ferrimagnetic ordering below T_c = 275 K with a Weiss constant $\theta = -750$ K and a frustration parameter of only 2.7 ($f = \theta/T_c$), a value significantly lower than those usually observed for frustrated compounds (f = 5−10).[46]

Let us now move on to compounds containing magnetic ladders. When studying **series 2**, we discovered $Ti_9Fe_2Ru_{18}B_8$ ($Zn_{11}Rh_{18}B_8$-type) in which Fe ladders were observed for the first time in intermetallic systems.[36] We were then able to synthesize more than a dozen of similar compounds, $Ti_9M_2Ru_{18}B_8$ (M = Cr, Mn, Co, Ni, Zn)[47] and the substitutional variants $Ti_{9-x}M_{2+x}Ru_{18}B_8$ (M = Cr, Mn, Co, Ni; x = 0−2).[48] Experimental investigations confirmed $Ti_9Fe_2Ru_{18}B_8$ as the first Ru-rich ferromagnet (T_C = 200 K), and theory identified spin-triplet Fe_2 dimers that are ferromagnetically coupled with neighboring Fe_2 dimers along the c-axis (Fe-ladder) to account for the unexpected magnetic behavior. Increasing the Fe-content by substituting Fe for Ti (adjacent to the Fe-ladder) induced a new Fe-substructure, the Fe-scaffold in $Ti_8Fe_3Ru_{18}B_8$ and $Ti_7Fe_4Ru_{18}B_8$,[37a] leading to a change of magnetic ordering from ferro- to ferrimagnetic. These experimental results were also well reproduced by the rigid band approximation combined with total energy calculations of several magnetic models for hypothetical $Ti_6Fe_5Ru_{18}B_8$, thus enabling the prediction of magnetic ordering depending on the VEC only: ferromagnetism (220 ≤ VEC < 223) and ferrimagnetism (VEC ≥ 223) were predicted,[37b] which is in exceptional agreement with the experimental results.[36,37a] Paramagnetism and thermoelectric properties have also been reported for these phases.[48,49]

The discovery of $FeRh_6B_3$ and $CoRh_6B_3$ as the first ferromagnetic borides (T_c = 225 and 150 K, respectively)[50−52] adopting the Th_7Fe_3 structure type provided new systems suitable for magnetic properties tuning. Furthermore, ferrimagnetic behavior (T_c = 5 K, with strong antiferromagnetic interactions) was found for $Fe_{0.5}Ru_{6.5}B_3$.[1b] These findings also support the above-mentioned theoretical discovery that Rh-rich borides containing Fe favor ferromagnetic interactions whereas Ru-rich phases favor antiferromagnetic interactions. Furthermore, investigations of the $FeRh_{6-x}Ru_xB_3$[53] and $CoRh_{6-x}Ru_xB_3$[54] series indeed show greater ferromagnetic interactions in the Rh-rich side of each series, as exemplified by the total magnetic moment, which linearly decreases with increasing Ru-content from 3.35 μ_B ($FeRh_5RuB_3$) to 0.70 μ_B ($FeRhRu_5B_3$).[53] As demonstrated by the paramagnetic series $CrRh_{6-x}Ru_xB_3$[55] and $NiRh_{6-x}Ru_xB_3$,[54] however, magnetic ordering is only possible in a given quaternary series if the parent ternary was already magnetically ordered.

4. CONCLUSIONS AND PERSPECTIVES

In this Account, we have demonstrated how computational methods can be effectively used to understand experimental discoveries (new crystal structures and itinerant magnetic properties) and predict new synthetic targets by selectively substituting atoms in many isostructural metal-rich borides. The rigid-band model, a simplified but still very useful way to analyze changes due to valence electron count (VEC) variation, turned out to be very helpful to understand and predict new isostructural metal-rich borides. For a more precise analysis, it was important to analyze the electronic density of states (DOS) together with chemical bonding using the COHP method. By changing the VEC, the position of the Fermi level (E_F) is adjusted with respect to the energy of the bands by taking advantage of the available pseudogap. We could understand the magnetic behavior of chains, ladders, scaffolds, and chains of triangles of magnetically active elements in different metallic and boron environments, as well as predict new synthetic targets. We could show that rational design is possible for itinerant magnets by systematically varying the magnetic properties (magnetic interactions and coercive fields) of seven different boride series. Using less expensive transition metals, we have predicted new itinerant magnets, the experimental proof of which is still pending. Moreover, several new structures have been discovered, all of which are being studied experimentally and computationally with the aim of finding new superconductors, magnets, and mechanically hard materials. Recently, we have also started to intensively study these borides experimentally and theoretically for their electrocatalytic properties, and the first results suggest a bright future for these materials.[56]

■ AUTHOR INFORMATION

Corresponding Author

*E-mail: bfokwa@ucr.edu. Website: www.fokwalab.ucr.edu.

ORCID

Boniface P. T. Fokwa: 0000-0001-9802-7815

Author Contributions

#J.P.S. and Y.Z. contributed equally.

Notes

The authors declare no competing financial interest.

Biographies

Jan P. Scheifers obtained his B.S. and M.S. in materials science at RWTH Aachen University (Germany) in 2014. After a short research experience at RWTH, he started his Ph.D. in the Fokwa group at University of California, Riverside, in 2016. His research focuses on experimental solid state chemistry of complex crystalline solids, specifically the syntheses of metal-rich borides and diffraction methods.

Yuemei Zhang received her B.S. and M.S. from Shandong University (China) and her Ph.D. from North Carolina State University in 2011. After a postdoctoral stay at Iowa State University, she joined the Fokwa group at University of California, Riverside, in 2015. Her main research interests are in electronic, magnetic, and electrocatalytic properties of intermetallics and oxides.

Boniface P. T. Fokwa obtained his B.S. and M.S. from University of Yaounde I (Cameroon), his Ph.D. from Dresden University of Technology (Germany), and his Habilitation from RWTH Aachen University (Germany). After working as Heisenberg Fellow at RWTH, he accepted an assistant Professor position at University of California, Riverside, in September 2015. His research group combines experimental and computational methods to rationally design materials

DOI: 10.1021/acs.accounts.7b00268
Acc. Chem. Res. 2017, 50, 2317−2325

for energy-related applications, such as magnets, superconductors, and electrocatalysts.

■ ACKNOWLEDGMENTS

The authors thank Deutsche Forschungsgemeinschaft (DFG), UC Riverside (startup fund to B.P.T.F.), and the National Science Foundation (Career award to B.P.T.F., No. DMR-1654780) for financial support. We thank all current and former Fokwa group members and all collaborators (especially Prof. Gordon J. Miller, ISU) for their contributions to the success of this research.

■ REFERENCES

(1) (a) Fokwa, B. P. T. Borides: Solid-state chemistry. In *Encyclopedia of Inorganic and Bioinorganic chemistry*; Scott, R. A., Ed.; John Wiley & Sons, Ltd., 2014. (b) Fokwa, B. P. T. Transition-metal-rich borides − fascinating crystal structures and magnetic properties. *Eur. J. Inorg. Chem.* **2010**, *2010*, 3075−3092.
(2) Albert, B.; Hillebrecht, H. Boron: Elementary challenge for experimenters and theoreticans. *Angew. Chem., Int. Ed.* **2009**, *48*, 8640−8668.
(3) (a) Mori, T. Boron-based materials. In *Materials aspect of thermoelectricity*; Uher, C., Ed.; CRC Press, 2016. (b) Akopov, G.; Yeung, M. T.; Kaner, R. B. Rediscovering the crystal chemistry of borides. *Adv. Mater.* **2017**, *29*, 1604506.
(4) Wong, J.; Tanaka, T.; Rowen, M.; Schäfers, F.; Müller, B. R.; Rek, Z. U. YB_{66} − a new soft x-ray monochromator for synchrotron radiation. II. Characterization. *J. Synchrotron Radiat.* **1999**, *6*, 1086−1095.
(5) Lafferty, J. M. Boride cathodes. *J. Appl. Phys.* **1951**, *22*, 299−309.
(6) Nagamatsu, J.; Nakagawa, N.; Muranaka, T.; Zenitani, Y.; Akimitsu, J. Superconductivity at 39 K in magnesium diboride. *Nature* **2001**, *410*, 63−64.
(7) Tan, X.; Chai, P.; Thompson, C. M.; Shatruk, M. Magnetocaloric effect in $AlFe_2B_2$: Toward magnetic refrigerants from earth-abundant elements. *J. Am. Chem. Soc.* **2013**, *135*, 9553−9557.
(8) Herbst, J. F.; Croat, J. J.; Pinkerton, F. E.; Yelon, W. B. Relationships between crystal structure and magnetic properties in $Nd_2Fe_{14}B$. *Phys. Rev. B: Condens. Matter Mater. Phys.* **1984**, *29*, 4176−4178.
(9) Svanidze, E.; Wang, J. K.; Besara, T.; Liu, L.; Huang, Q.; Siegrist, T.; Frandsen, B.; Lynn, J. W.; Nevidomskyy, A. H.; Gamża, M. B.; Aronson, M. C.; Uemura, Y. J.; Morosan, E. An itinerant antiferromagnetic metal without magnetic constituents. *Nat. Commun.* **2015**, *6*, 7701.
(10) Villars, P. Pearsons's Handbook: Crystallographic data for intermetallic phases. ASM International: Materals Park, OH, 1997.
(11) Fokwa, B. P. T.; Hermus, M. Complete titanium substitution by boron in a tetragonal prism: Exloring the complex borides series $Ti_{3-x}Ru_{5-y}Ir_yB_{2+x}$ ($0 \le x \le 1$ and $1 < y < 3$) by experiment and theory. *Inorg. Chem.* **2011**, *50*, 3332−3341.
(12) Ade, M.; Hillebrecht, H. Ternary borides Cr_2AlB_2, Cr_3AlB_4, and Cr_4AlB_6: The first members of the series $(CrB_2)_nCrAl$ with n = 1, 2, 3 and a unifying concept for ternary borides as MAB-phases. *Inorg. Chem.* **2015**, *54*, 6122−6135.
(13) Mbarki, M.; St. Touzani, R.; Fokwa, B. P. T. Experimental and theoretical inverstigation of the ternary boride NbRuB with a layerlike strucuture type. *Eur. J. Inorg. Chem.* **2014**, *2014*, 1381−1388.
(14) Mbarki, M.; St. Touzani, R.; Fokwa, B. P. T. Nb_2OsB_2, with a new twofold superstructure of the U_3Si_2 type: Synthesis, crystal chemistry and chemical bonding. *J. Solid State Chem.* **2013**, *203*, 304−309.
(15) Jedlicka, H.; Benesovsky, F.; Nowotny, H. Die Kristallstruktur des W_3CoB_3 und der dazu isotypen Phasen Mo_3CoB_3, Mo_3NiB_3 und W_3NiB_3. *Monatsh. Chem.* **1969**, *100*, 844−850.
(16) Rogl, P.; Benesovsky, F.; Nowotny, H. Über einige Komplexboride mit Platinmetallen. *Monatsh. Chem.* **1972**, *103*, 965−989.
(17) Malik, Z. P.; Sologub, O.; Grytsiv, A.; Giester, G.; Rogl, P. F. Crystal structure of novel Ni-Zn borides: First observation of a boron-metal nested cage unit: $B_{20}Ni_6$. *Inorg. Chem.* **2011**, *50*, 7669−7675.
(18) Goerens, C.; Fokwa, B. P. T. The complex metal-rich boride $Ti_{1+x}Rh_{2-x+y}Ir_{3-y}B_3$ (x = 0.68, y = 1.06) with a new structure type containing B_4 zigzag fragments: Synthesis, crystal chemistry and theoretical calculations. *J. Solid State Chem.* **2012**, *192*, 113−119.
(19) Kotzott, D.; Ade, M.; Hillebrecht, H. Synthesis and crystal structures of α- and β-modifications of Cr_2IrB_2 containing 4-membered B_4 chain fragments, the τ-boride $Cr_{7.9}Ir_{14.1}B_6$ and orthorhombic Cr_2B. *Solid State Sci.* **2008**, *10*, 197−302.
(20) Fokwa, B. P. T.; von Appen, J.; Dronskowski, R. Synthesis of a missing structure link: The first trigonal planar B_4 units in the novel complex boride $Ti_{1+x}Os_{2-x}RuB_2$ (x = 0.6). *Chem. Commun.* **2006**, 4419−4421.
(21) Noläng, B. I.; Tergenius, L.-E.; Westman, I. The crystal structure of Rh_5B_4. *J. Less-Common Met.* **1981**, *82*, 303−308.
(22) Hillebrecht, H.; Ade, M. B_4 tetrahedra for aluminum atoms- a surprising substitution in τ-borides $Ni_{20}Al_3B_6$ and $Ni_{20}AlB_{14}$. *Angew. Chem., Int. Ed.* **1998**, *37*, 935−938.
(23) Ade, M.; Kotzott, D.; Hillebrecht, H. Sythesis and crystal structures of the new metal-rich ternary borides $Ni_{12}AlB_8$, $Ni_{12}GaB_8$, and $Ni1_{0.6}Ga_{0.4}B_6$—examples for the first B_5 zig-zag chain fragment. *J. Solid State Chem.* **2010**, *183*, 1790−1797.
(24) Fokwa, B. P. T.; Hermus, M. All-boron planar B_6 ring in the solid-state phase $Ti_7Rh_4Ir_2B_8$. *Angew. Chem., Int. Ed.* **2012**, *51*, 1702−1705.
(25) Zheng, Q.; Kohout, M.; Gumeniuk, R.; Abramchuk, N.; Borrmann, H.; Prots, Y.; Burkhardt, U.; Schnelle, W.; Akselrud, L.; Gu, H.; Leithe-Jasper, A.; Grin, Y. $TM_7TM'_6B_8$ (TM = Ta, Nb; TM′ = Ru, Rh, Ir): New compounds with $[B_6]$ ring polyanions. *Inorg. Chem.* **2012**, *51*, 7472−7483.
(26) Mbarki, M.; St. Touzani, R.; Fokwa, B. P. T. Unexpected synergy between magnetic iron chains and stacked B_6 rings in $Nb_6Fe_{1-x}Ir_{6+x}B_8$. *Angew. Chem., Int. Ed.* **2014**, *53*, 13174−13177.
(27) Zheng, Q.; Gumeniuk, R.; Borrmann, H.; Schnelle, W.; Tsirlin, A. A.; Rosner, H.; Burkhardt, U.; Reissner, M.; Grin, Y.; Leithe-Jasper, A. Ternary borides $Nb_7Fe_3B_8$ and $Ta_7Fe_3B_8$ with kagome-type iron framework. *Dalton, Trans.* **2016**, *45*, 9590−9600.
(28) Li, W.-L.; Xie, L.; Jian, T.; Romanescu, C.; Huang, X.; Wang, L.-S. (2014), Hexagonal Bipyramidal $[Ta_2B_6]^{-/0}$ Clusters: B_6 Rings as Structural Motifs. *Angew. Chem., Int. Ed.* **2014**, *53*, 1288−1292 and references therein.
(29) Landrum, G. A.; Dronskowski, R. The orbital origins of magnetism: From atoms to molecules to ferromagnetic alloys. *Angew. Chem., Int. Ed.* **2000**, *39*, 1560−1585.
(30) Gourdon, O.; Gout, D.; Miller, G. J. Electronic states of intermetallic compounds. In *Encyclopedia of Condensed Matter Physics*; Bassani, F., Liedl, G. L., Wyder, P., Eds.; Elsevier: Oxford, 2005, pp 409−422.
(31) Mbarki, M.; St. Touzani, R.; Rehorn, W. G.; Gladisch, F. C.; Fokwa, B. P. T. New ternary tantalum borides containing boron dumbbells: Experimental and theoretical studies of Ta_2OsB_2 and TaRuB. *J. Solid State Chem.* **2016**, *242*, 28−33.
(32) Hermus, M.; Fokwa, B. P. T. Experimental and first-principle studies of the ternary borides $Ta_3Ru_5B_2$ and $M_{3-x}Ru_{5+x}B_2$ (M = Zr, Hf). *Eur. J. Inorg. Chem.* **2014**, *2014*, 3085−3094.
(33) St. Touzani, R.; Fokwa, B. P. T. Electronic, structure and magnetic studies of niobium borides of group 8 transition metals, Nb_2MB_2 (M = Fe, Ru, Os) from first principle calculations. *J. Solid State Chem.* **2014**, *211*, 227−234.
(34) St. Touzani, R.; Rehorn, C. W. G.; Fokwa, B. P. T. Influence of chemical bonding and magnetism on elastic properties of the A_2MB_2 borides (A = Nb, Ta; M = Fe, Ru, Os) from first-principle calculations. *Comput. Mater. Sci.* **2015**, *104*, 52−59.

DOI: 10.1021/acs.accounts.7b00268
Acc. Chem. Res. 2017, 50, 2317−2325

(35) Fokwa, B. P. T.; Lueken, H.; Dronskowski, R. Rational synthetic tuning between itinerant antiferromagnetism and ferromagnetism in the complex boride series $Sc_2FeRu_{5-n}Rh_nB_2$ ($0 \leq n \leq 5$). *Chem. - Eur. J.* **2007**, *13*, 6040−6046.
(36) Fokwa, B. P. T.; Samolyuk, G. D.; Miller, G. J.; Dronskowski, R. Ladders of a magnetically active element in the structure of the novel complex boride $Ti_9Fe_2Ru_{18}B_8$: Synthesis, structure, bonding, and magnetism. *Inorg. Chem.* **2008**, *47*, 2113−2120.
(37) (a) Goerens, C.; Brgoch, J.; Miller, G. J.; Fokwa, B. P. T. Scaffolding, Ladders, Chains, and Rare Ferrimagnetism in Intermetallic Borides: Synthesis, Crystal Chemistry and Magnetism. *Inorg. Chem.* **2011**, *50*, 6289−6296. (b) Brgoch, J.; Goerens, C.; Fokwa, B. P. T.; Miller, G. J. Scaffolding, ladders, chains, and rare ferrimagnetism in intermetallic borides: Electronic structure calculations and magnetic ordering. *J. Am. Chem. Soc.* **2011**, *133*, 6832−6840.
(38) Küpers, M.; Lutz-Kappelman, L.; Zhang, Y.; Miller, G. J.; Fokwa, B. P. T. Spin frustration and magnetic ordering from one-dimensional stacking of Cr_3 triangles in $TiCrIr_2B_2$. *Inorg. Chem.* **2016**, *55*, 5640−5648.
(39) Nagelschmitz, E. A.; Jung, W.; Feiten, R.; Müller, P.; Lueken, H. Ternary rhodium borides $A_3Rh_5B_2$ (A = Mag, Sc) and quaternary derivatives $A_2MRh_5B_2$. Preparation, crystal stucture (M = main group and 3*d* elementes), and magnetism (M = Mn, Fe). *Z. Anorg. Allg. Chem.* **2001**, *627*, 523−532.
(40) Fokwa, B. P. T. Valence-electron-driven Ru/Ti site preference in the new ternary boride $Ti_{10}Ru_{19}B_8$: Synthesis and single-crystal structure refinement. *Z. Anorg. Allg. Chem.* **2009**, *635*, 2258−2262.
(41) Samolyuk, G. D.; Fokwa, B. P. T.; Dronskowski, R.; Miller, G. J. Electronic structure, chemical bonding, and magnetic properties in the intermetallic series $Sc_2Fe(Ru_{1-x}Rh_x)_5B_2$ from first principle. *Phys. Rev. B* **2007**, *76*, 094404.
(42) Brgoch, J.; Mahmoud, A.; Miller, G. J. Atomic site preference and its effect on magnetic structure in the intermetallic borides $M_2Fe(Ru_{0.8}T_{0.2})_5B_2$ (M = Sc, Ti, Zr; T = Ru, Rh, Ir). *J. Solid State Chem.* **2012**, *196*, 168−174.
(43) Hermus, M.; Yang, M.; Grüner, D.; DiSalvo, F. J.; Fokwa, B. P. T. Drastic change of magnetic interactions and hysteresis through site-preferential Ru/Ir substitution in $Sc_2FeRu_{5-x}Ir_xB_2$. *Chem. Mater.* **2014**, *26*, 1967−1974.
(44) Fokwa, B. P. T.; Lueken, H.; Dronskowski, R. Rational design of complex boride − one-electon-step evolution from soft to semi-hard itinerant ferromagnets in the new boride series $Ti_2FeRu_{5-n}Rh_nB_2$ ($1 \leq n \leq 5$). *Eur. J. Inorg. Chem.* **2011**, *2011*, 3926−3930.
(45) Zhang, Y.; Miller, G. J.; Fokwa, B. P. T. Computational design of rare-earth-free magnets with the $Ti_3Co_5B_2$-type structure. *Chem. Mater.* **2017**, *29*, 2535−2541.
(46) Zhu, T.-T.; Sun, W.; Huang, Y.-X.; Sun, Z.-M.; Pan, Y.; Balents, L.; Mi, J. X. Strong spin frustration from isolated triangular Cu(II) trimers in $SrCu(OH)_3Cl$ with a novel cuprate layer. *J. Mater. Chem. C* **2014**, *2*, 8170−8178.
(47) Fokwa, B. P. T.; Goerens, C.; Gilleßen, M. New quaternary complex borides, $Ti_9M_2Ru_{18}B_8$ (Cr, Mn, Co, Ni, Cu, Zn): Synthesis, crystal structure and bonding analysis. *Z. Kristallogr. - Cryst. Mater.* **2010**, *225*, 180−186.
(48) Goerens, C.; Brgoch, J.; Miller, G. J.; Fokwa, B. P. T. Scaffolds of magnetically active 3*d* metals in the valence electron controlled borides $Ti_{9-x}M_{2+x}Ru_{18}B_8$ (M = Cr−Ni; x = 0.5−1): Structural, electronic and magnetic properties. *J. Solid State Chem.* **2013**, *204*, 283−290.
(49) Takagiwa, Y.; Yoshida, T.; Yanagihara, D.; Kimura, K. Thermoelectric properties of pseudogap $Ti_{10}Ru_{19}B_8$ and $Ti_9TM_2Ru_{18}B_8$ (TM: Cr-Cu) compounds. *J. Electron. Mater.* **2015**, *44*, 1483−1490.
(50) Fokwa, B. P. T.; Dronskowski, R. Synthesis, crystal structure determinnation and Fe/Rh site preference in the new ternary boride $FeRh_6B_3$. *Z. Anorg. Allg. Chem.* **2005**, *631*, 2478−2480.
(51) Ndassa, I. M.; Gilleβen, M.; Fokwa, B. P. T. Electronic structure, chemical bonding and magnetism of the metal-rich borides MRh_6B_3 (M = Cr, Mn, Fe, Co, Ni) with Th_7Fe_3-type structure: A density functional theory study. *Solid State Sci.* **2013**, *17*, 14−20.
(52) Misse, P. R. N.; Gilleβen, M.; Fokwa, B. P. T. Site-preferential design of itinerant ferromagnetic borides: Experimental and theoretical investigation of MRh_6B_3 (M = Fe, Co). *Inorg. Chem.* **2011**, *50*, 10303−10309.
(53) Shankhari, P.; Misse, P. R. N.; Mbarki, M.; Park, H.; Fokwa, B. P. T. Chemical tuning of magnetic properties through Ru/Rh substitution in Th_7Fe_3-type $FeRh_{6-n}Ru_nB_3$ (n = 1−5) series. *Inorg. Chem.* **2017**, *56*, 446−451.
(54) Park, H.; Misse, P. R. N.; Mbarki, M.; Shankhari, P.; Fokwa, B. P. T. Synthesis and magnetic properties of the new boride series $MRh_{6-n}Ru_nB_3$ (M = Co, Ni; n = 1−5). *Eur. J. Inorg. Chem.* **2017**, DOI: 10.1002/ejic.201700418.
(55) Misse, P. R. N.; Mbarki, M.; Fokwa, B. P. T. Synthesis, crystal structure investigation and magnetism of the complex metal-rich boride series $Cr_x(Rh_{1-y}Ru_y)_{7-x}B_3$ (x = 0.88−1; y = 0−1) with Th_7Fe_3-type structure. *J. Solid State Chem.* **2012**, *192*, 331−336.
(56) Park, H.; Encinas, A.; Scheifers, J. P.; Zhang, Y.; Fokwa, B. P. T. Boron-dependency of molybdenum borides electrocatalysts for the hydrogen evolution reaction. *Angew. Chem., Int. Ed.* **2017**, *56*, 5575−5578.

DOI: 10.1021/acs.accounts.7b00268
Acc. Chem. Res. 2017, 50, 2317−2325